Supplement of Atmos. Chem. Phys., 22, 7461–7487, 2022
https://doi.org/10.5194/acp-22-7461-2022-supplement
© Author(s) 2022. CC BY 4.0 License.

Supplement of

Satellite soil moisture data assimilation impacts on modeling weather variables and ozone in the southeastern US – Part 2: Sensitivity to dry-deposition parameterizations

Min Huang et al.

Correspondence to: Min Huang (mhuang10@gmu.edu)

The copyright of individual parts of the supplement might differ from the article licence.

Table S1. The original 20 Land Use Land Cover (LULC) types for WRF-Chem simulations and the criteria applied to group them for analysis.

LULC Category	LULC Description[a]	Grouped LULC type shown in Figure 1
1	Evergreen Needleleaf Forest	Forests
2	Evergreen Broadleaf Forest	
3	Deciduous Needleleaf Forest	
4	Deciduous Broadleaf Forest	
5	Mixed Forests	
6	Closed Shrublands	Shrub/Grass
7	Open Shrublands	
8	Woody Savannas	
9	Savannas	
10	Grasslands	
11	Permanent Wetlands	
12	Croplands	Croplands
13	Urban and Built-Up	Urban
14	Cropland/Natural Vegetation Mosaic	Croplands
15	Snow and Ice	Water and others
16	Barren or Sparsely Vegetated	
17	Water	
18	Wooded Tundra	
19	Mixed Tundra	
20	Barren Tundra	

[a]Sources:
https://www2.mmm.ucar.edu/wrf/users/docs/user_guide_V3/user_guide_V3.9/users_guide_chap3.html#_Land_Use_and
https://www2.mmm.ucar.edu/wrf/users/download/get_sources_wps_geog.html
Last access: 26 March 2022

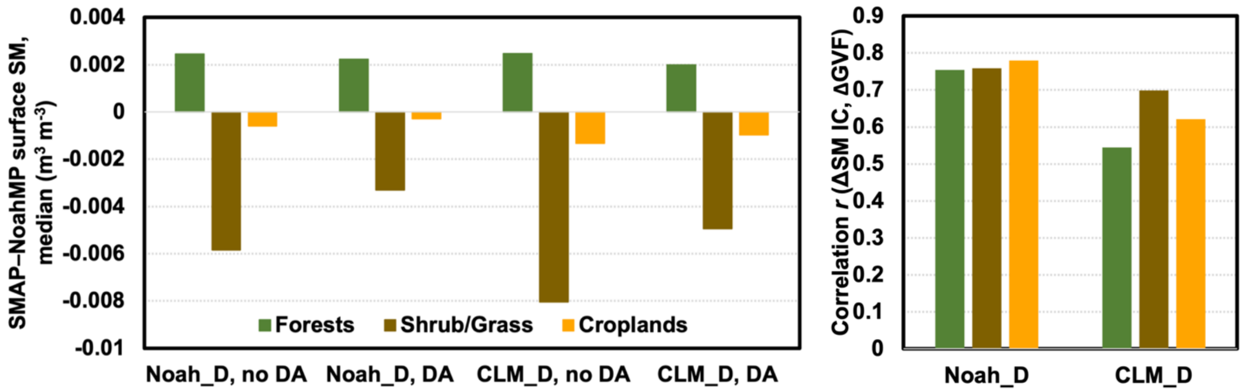

Figure S1: (left) Surface soil moisture (SM) differences between SMAP and Noah-MP, and (right) correlation coefficient *r* values between the period-mean, SM initial condition changes and green vegetation fraction responses to the SM data assimilation, summarized by three LULC groups.

In Noah-MP, leaf carbon mass C_{leaf}, from which leaf area and green vegetation fraction are converted, is computed based on equation (10) in Niu et al. (2011):

$$\frac{\partial C_{leaf}}{\partial t} = F_{leaf}A - (S_{cd} + T_{leaf} + R_{leaf})C_{leaf}$$

where A is the total carbon assimilation rate of the sunlit and shaded leaves. F_{leaf}, S_{cd}, T_{leaf}, and R_{leaf}, all of which have LULC dependencies, represent the fraction of the assimilated carbon allocated to leaf, the death rate due to cold and water stresses, the leaf turnover rate, and the leaf respiration rate, respectively. The leaf death rate due to water stress and the leaf respiration rate are functions of water stress coefficient which is determined based on the SM factor controlling stomatal resistance (i.e., β factor). The applied β scheme in Noah-MP, therefore, affects the modeled SM-vegetation growth relationships and the vegetation responses to the SM data assimilation.

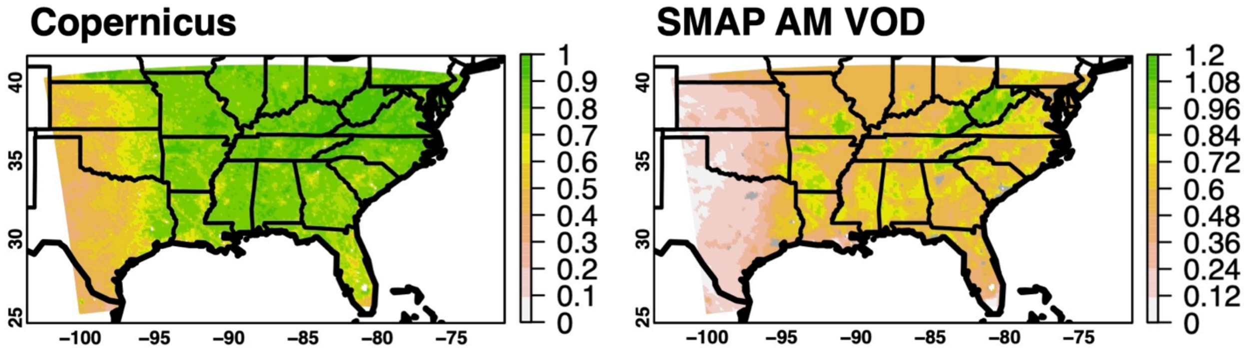

Figure S2: August 2015-2019 (left) green vegetation fraction (GVF) from a 10-day average Copernicus Global Land Service product which is computed from leaf area index and other canopy structural variables and (right) SMAP morning-time (AM) vegetation optical depth (VOD) climatology. Grey indicates missing data over terrestrial regions.

Assuming that GVF and VOD anomalies are similar, the satellite-based, period-mean GVF data shown in Figure 2a were estimated using the following approach:

For each model grid (i,j),

$$\text{Derived GVF}\,(\mathbf{i},\mathbf{j}) = \frac{\text{SMAP AM VOD, period mean}\,(\mathbf{i},\mathbf{j})}{\text{SMAP AM VOD climatology}\,(\mathbf{i},\mathbf{j})} \times \text{Copernicus GVF climatology}\,(\mathbf{i},\mathbf{j})$$

Any derived GVF values exceeding 1.0 are considered invalid and not used.

The accuracy of the satellite-derived GVF fields can be affected by: 1) the quality of the original Copernicus GVF product, which has an overall slight positive bias of 0.02 (4.0%) relative to ground-based observations, and such biases are land cover dependent (Copernicus Global Land Operations, 2020); 2) the uncertainty in the original SMAP VOD retrievals, which may be reduced or canceled as the ratios of period-mean/climatological VOD were applied in the calculation; 3) the temporal representativeness of the 10-day average Copernicus GVF product as the land surface conditions under cloudy and poor atmospheric conditions cannot be sampled; and 4) this approach used to derive the period-mean GVF and the assumptions associated with it. In the discussions in Section 3.1, we assume that 1) is the main source of uncertainty of these satellite-derived GVF fields, and according to Copernicus Global Land Operations (2020), positive biases are very likely to be associated with the GVF data exceeding 0.6 over forests and croplands and those falling within 0.2−0.6 over grasslands.

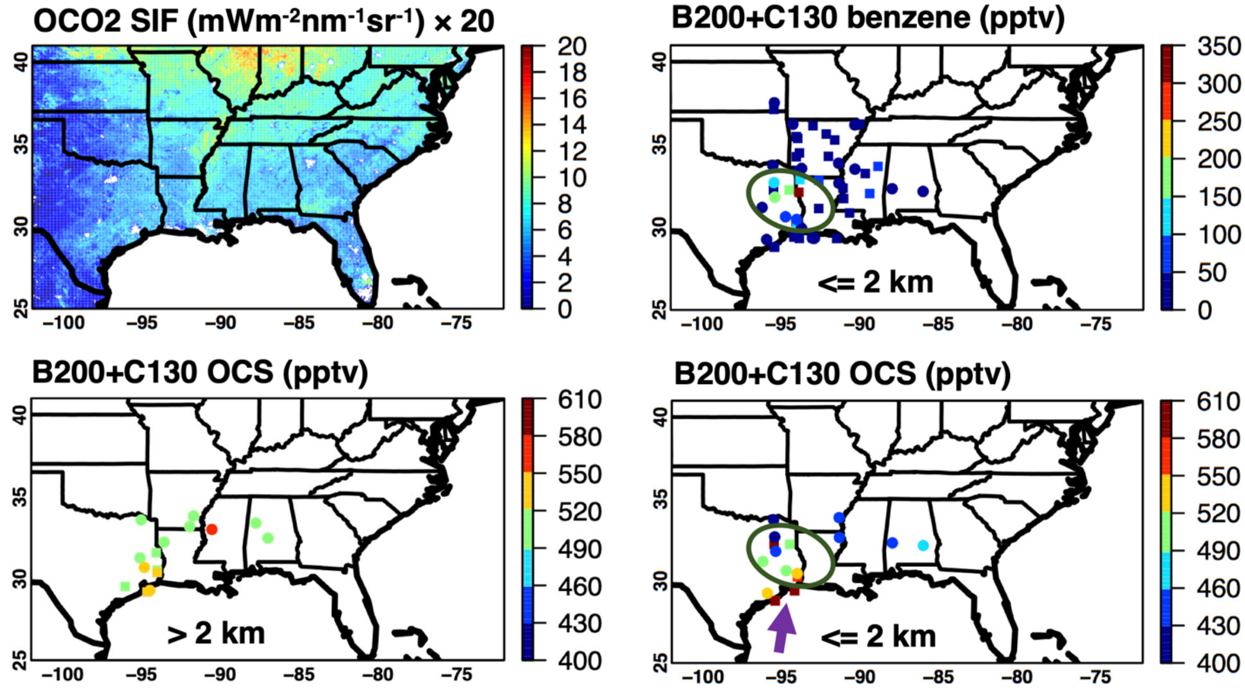

Figure S3: Proxies of gross primary productivity: (upper left) solar-induced chlorophyll fluorescence (SIF) data derived from the Orbiting Carbon Observatory-2 data during mid–late August 2021, scaled by 20; (lower) carbonyl sulfide (OCS) data during the 2016 ACT-America campaign, taken onboard the B-200 and C-130 aircraft at different altitudes; (upper right) near-surface benzene measured onboard the B-200 and C-130 aircraft during ACT-America, used to indicate influences of combustion sources. Filled squares and circles indicate B-200 and C-130 data, respectively. The green circles in the right panels highlight the collocated benzene and OCS hotspots possibly affected by anthropogenic combustion sources in the eastern Texas which have been reported also in Zumkehr et al. (2018). The purple arrow in the lower right panel points to the OCS data likely affected by known oceanic emission sources (Lennartz et al., 2017). The maximum OCS mixing ratios of >550 pptv, and the maximum OCS drawdowns that far exceeded 60 pptv around the Lower Mississippi cropland regions and the Texas-Oklahoma border where soil was wet and likely an OCS source (Bunk et al., 2017), are much larger than those observed in summer 2004 over the eastern US (Campbell et al., 2008), indicating possible higher OCS emissions and stronger terrestrial carbon uptake in summer 2016 than in summer 2004.

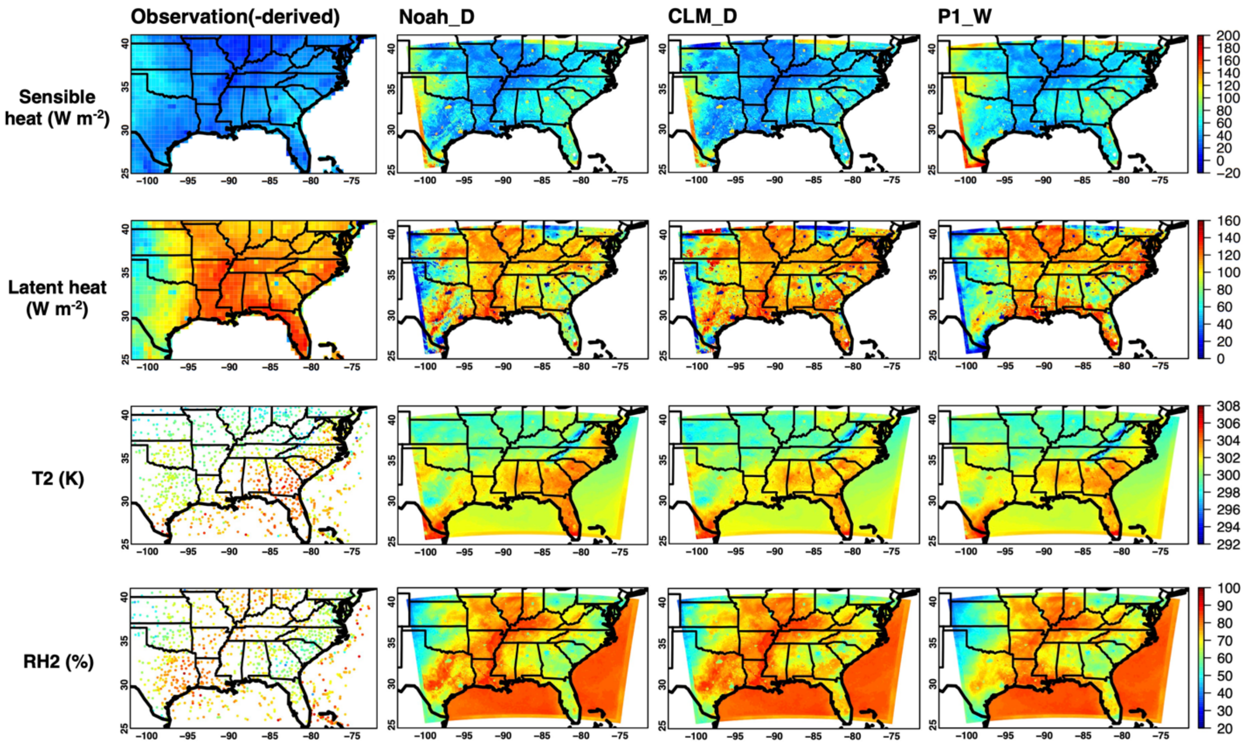

Figure S4: Period-mean (16–28 August 2016), model-based (from the Noah_D, CLM_D, and P1_W no-DA cases) sensible and latent heat fluxes, 2 m air temperature (T2) and humidity (RH2) in comparison with observational or observation-derived datasets (i.e., FLUXCOM, and the National Centers for Environmental Prediction Global Surface Observational Weather Data).

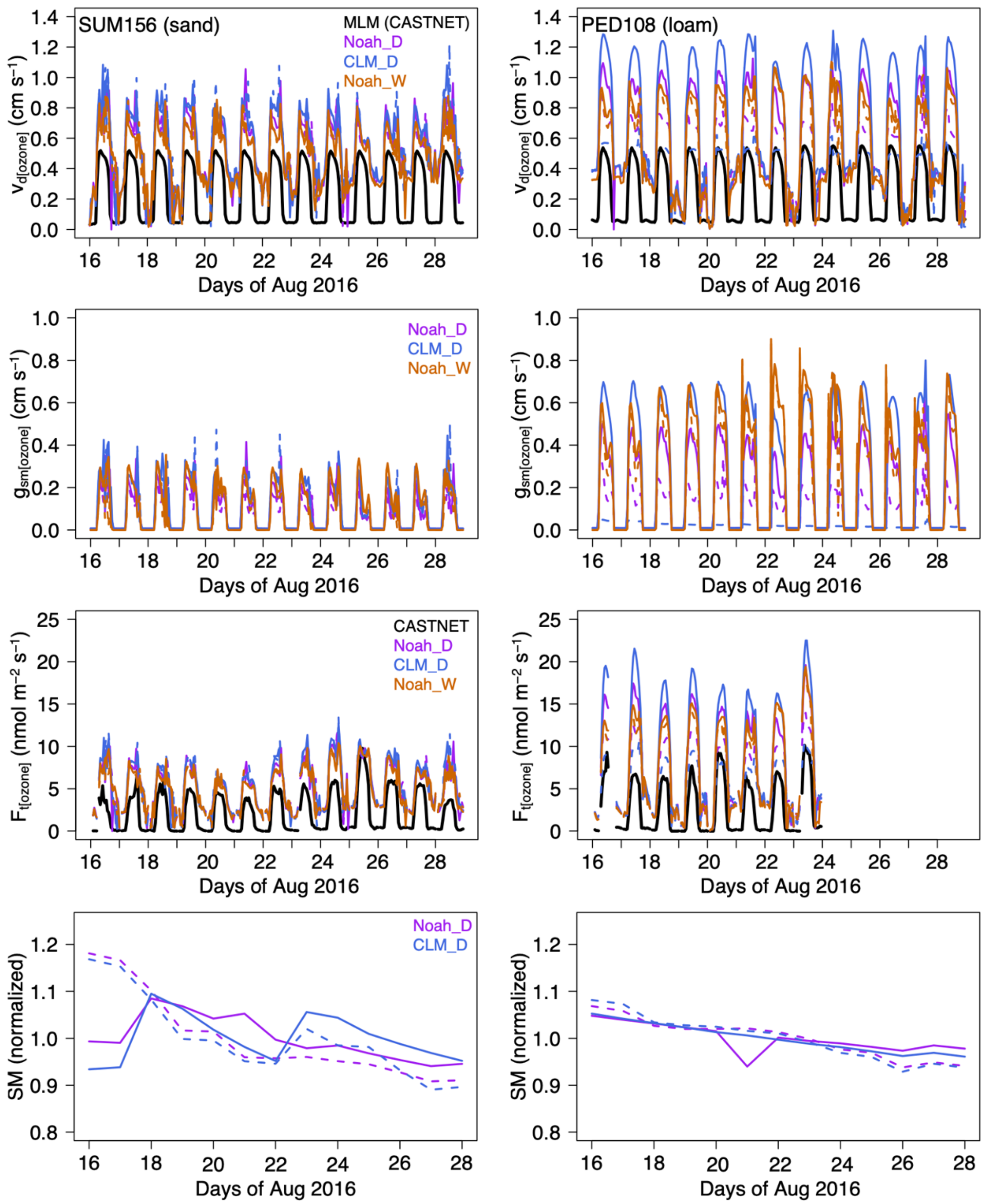

Figure S5: Time series of ozone dry deposition velocity v_d, stomatal-mesophyll conductance g_{sm}, ozone dry deposition flux F_t and the anomaly of column-averaged SM initial conditions relative to their period mean values during 16–28 August 2016, at the SUM156 and PED108 sites whose locations are shown in Figure 1d. The Clean Air Status and Trends Network (CASTNET) data are in black solid lines, and their WRF-Chem counterparts are in purple, blue and brown lines. The WRF-Chem results from the no-DA and DA cases are indicated in solid and dashed lines, respectively.

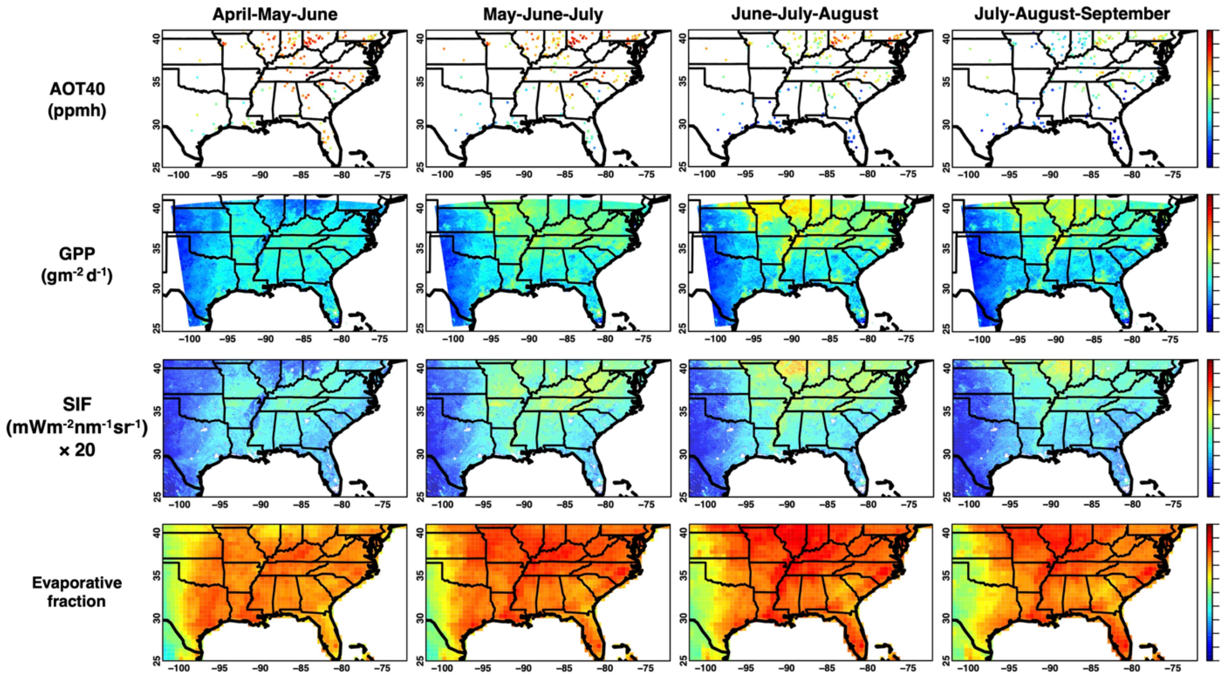

Figure S6: AOT40 in cropland-dominant model grids based on the Air Quality System and Clean Air Status and Trends Network surface ozone observations, SMAP level 4 carbon gross primary productivity (GPP), Orbiting Carbon Observatory-2 derived solar-induced chlorophyll fluorescence (SIF), scaled by 20, and FLUXCOM evaporative fraction, averaged for three consecutive months during 2016 growing seasons.

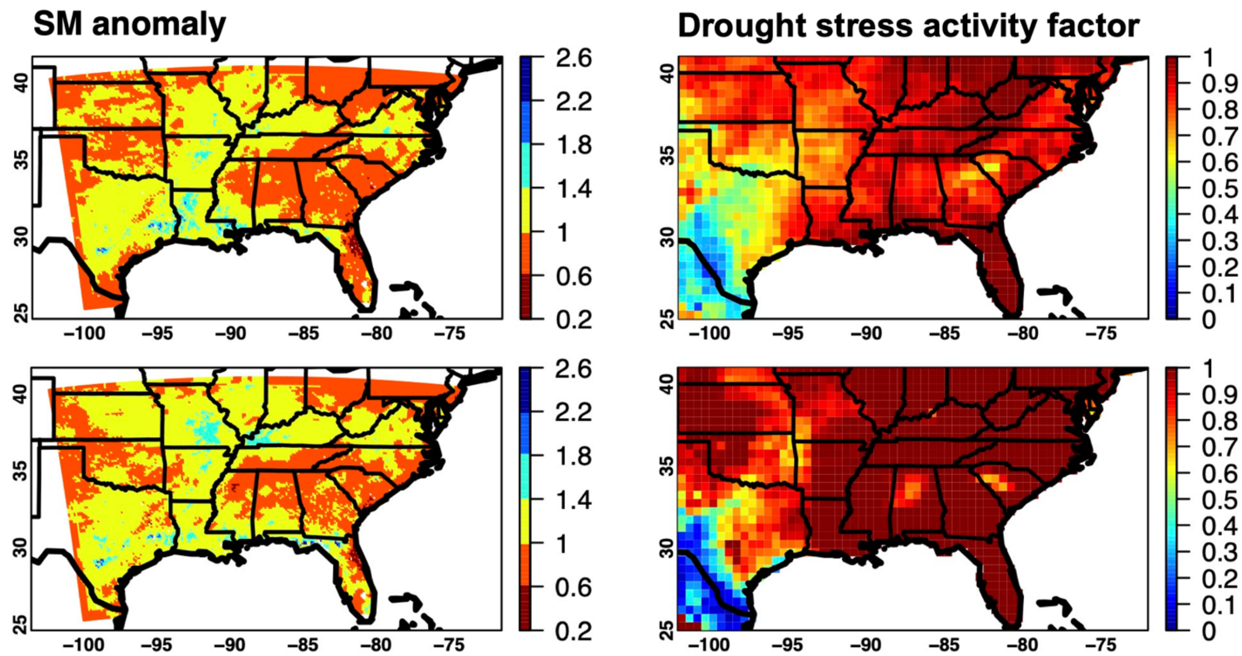

Figure S7: (left) Column-averaged soil moisture (SM) anomalies from the CLM_D case of this work, defined as the period-mean (16–28 August 2016) SM at WRF-Chem initial times divided by SM averaged through 00 UTC of the reference period; and (right) drought stress activity factor γ_d for biogenic isoprene emission calculations from Jiang et al. (2018) averaged for the reference period. Results are shown for reference periods of (upper) August 2005–2014 and (lower) August 2014.

The γ_d values east of 90 °W within our study domain are mostly >0.7 during the two reference periods. In August 2016, high biogenic isoprene emission regions, including the Missouri Ozarks, were wetter than the August 2005–2014 and August 2014 conditions and therefore for these regions the SM direct controls on biogenic isoprene emissions were weak. However, omitting the SM direct effects on biogenic isoprene emissions over several states that were experiencing drier-than-normal soil conditions, particularly South Carolina, Georgia, and Alabama, may introduce relatively larger uncertainty to biogenic emission and ozone modeling.

References

Bunk, R., Behrendt, T., Yi, Z., Andreae, M. O., and Kesselmeier, J.: Exchange of carbonyl sulfide (OCS) between soils and atmosphere under various CO_2 concentrations, J. Geophys. Res. Biogeosci., 122, 1343–1358, https://doi.org/10.1002/2016JG003678, 2017.

Campbell, J. E., Carmichael, G. R., Chai, T., Mena-Carrasco, M., Tang, Y., Blake, D. R., Blake, N. J., Vay, S. A., Collatz, G. J., Baker, I., Berry, J. A., Montzka, S. A., Sweeney, C., Schnoor, J. L., and Stanier, C. O.: Photosynthetic control of atmospheric carbonyl sulfide during the growing season, Science, 322, 1085–1088, https://doi.org/10.1126/science.1164015, 2008.

Copernicus Global Land Operations: Scientific Quality Evaluation of LAI, FAPAR, FCOVER Collection 1 km, Version 1 & Version 2, I1.00, available at: https://land.copernicus.eu/global/sites/cgls.vito.be/files/products/CGLOPS1_SQE2019_LAI1km-V1%26V2_I1.00.pdf (last access: 28 March 2022), 2020.

Lennartz, S. T., Marandino, C. A., von Hobe, M., Cortes, P., Quack, B., Simo, R., Booge, D., Pozzer, A., Steinhoff, T., Arevalo-Martinez, D. L., Kloss, C., Bracher, A., Röttgers, R., Atlas, E., and Krüger, K.: Direct oceanic emissions unlikely to account for the missing source of atmospheric carbonyl sulfide, Atmos. Chem. Phys., 17, 385–402, https://doi.org/10.5194/acp-17-385-2017, 2017.

Niu, G. Y., Yang, Z. L., Mitchell, K. E., Chen, F., Ek, M. B., Barlage, M., Kumar, A., Manning, K., Niyogi, D., Rosero, E., Tewari, M., and Xia, Y.: The community Noah land surface model with multiparameterization options (Noah-MP): 1. Model description and evaluation with local-scale measurements, J. Geophys. Res.-Atmos., 116, 1–19, https://doi.org/10.1029/2010JD015139, 2011.

Zumkehr, A., Hilton, T. W., Whelan, M. E., Smith, S., Kuai, L., Worden, J., and Campbell, J. E.: Global Gridded Anthropogenic Emissions Inventory of Carbonyl Sulfide, Atmos. Environ., 183, 11–19, https://doi.org/10.1016/j.atmosenv.2018.03.063, 2018.